American Mineralogist, Volume 74, pages 191–199, 1989

Fluorescence spectra of Eu^{3+} in synthetic polycrystalline anorthite: Distribution of Eu^{3+} in the structure

Phillipe D'Arco

École normale Supérieure, Laboratoire de Géologie, 24, Rue Lhomond, 75231 Paris Cedex 05, France

Bernard Piriou

Laboratoire des Éléments de Transition dans les Solides, CNRS, 1, Place A. Briand, 92195 Meudon Principal Cedex, France

Abstract

The localization of the trivalent rare-earth-element ions (REE^{3+}) in synthetic polycrystalline anorthite is investigated by optical spectroscopy, using Eu^{3+} as a representative local probe. This ion is found either trapped in defects such as possibly twin and cleavage planes or substituted for Ca^{2+} in the structural sites. But the substitution of Eu^{3+} for Ca^{2+} is probably accompanied by deformation of the aluminosilicate framework, which results in the development of numerous additional sites that form three subsets, each related to an original site. Such a distribution may explain the low partition coefficients of REEs between plagioclases and magmatic liquids and the fact that the REE partition coefficients are independent of atomic number.

Introduction

A review of the literature clearly shows a lack of understanding of the mechanisms of incorporating or trapping of the rare-earth elements (REEs) in minerals, even for relatively high concentrations (1000 ppm). Proposed explanations are indirect. Harrison (1978, 1981) interpreted the incorporation of REEs in garnet and diopside by trapping them in point defects at low concentrations and by their substitution for the major elements at higher concentrations. Using a point-defect scheme, Morlotti and Ottonello (1982) have developed a model compatible with Harrison's interpretation and with the observed experimental distributions of REEs between minerals and liquids. However, the lack of direct evidence seriously limits our understanding of the relative distribution of the elements among the different phases during geochemical processes. As a consequence, several authors have tried to find some parameters (ionic radii, charge) numerically correlated with the partition coefficients to explain their variations (see Jensen, 1973; Morgan and Wandless, 1980). But direct evidence for any physical or chemical relationships is still missing.

Using different spectroscopic methods, at very high concentrations of REEs, several synthetic accessory minerals of industrial interest have been studied, e.g., zircon (Reynolds et al., 1972; Ball, 1982) and apatite (Fahmi, 1986; Piriou et al., 1987). But few data are available about the principal rock-forming minerals. This is true particularly of feldspars, despite their quantitative importance in geologic systems and their classical Eu anomaly. The only known study of the localization of REEs in feldspars is by Morris (1975). In his study of the EPR spectra of Eu^{2+} and Gd^{3+} in synthetic anorthite, he concluded that both ions occupy the Ca^{2+} sites; however, he could not differentiate between the different sites. The Eu^{2+} spectra display sharp transitions indicating well-defined ion sites. However, the Gd^{3+} spectra are similar to those of the same ion in glasses. Two interpretations of these glass-type spectra were proposed by Morris (1975): (1) Gd^{3+} substitutes for Ca^{2+} but displays positional disorder in the large Ca^{2+} sites, or (2) the incorporation of such a highly charged cation substituting for Ca^{2+} yields an increase of stress on the O–(Si,Al)–O angles and an "amorphization" of the structure around those cations by breakage of some O–(Si,Al) bonds.

In this article, we re-examine the trapping of REE^{3+} in anorthite on the basis of fluorescence spectra of Eu^{3+} chosen as a representative of the other REE^{3+} and used as a local probe of the crystal field. It is not our goal to explain the Eu anomaly of feldspars, which is only weakly developed in anorthite (relative to K-feldspars).

Method and experimental procedures

Method

Fluorescence spectra of REE^{3+} in solids give information about the crystal field exerted on these elements. The optical properties of the REE^{3+} ions involve only *f* electrons that are inner electrons shielded from external fields by two electronic outer shells. Consequently, these electrons are only weakly perturbed by the crystal field. Since the splittings are small, the terms and their levels remain easily identifiable for the REEs (see Caro, 1976). In contrast, the energetic structure of the *d*-transition metals is strongly perturbed by the crystal field. Because the splittings are large, the identification of the levels (and sometimes even of the terms) is difficult for the transition metals.

Among the REE^{3+}, Eu^{3+} is characterized by its ground-state level $^7F_0$ (notation $^{2S+1}L_J$) and its lower emitting level $^5D_0$ which both are nondegenerate. In the case of a free ion, the transitions between these two levels (noted $^5D_0 \rightarrow {}^7F_0$ (emission) or $^7F_0 \rightarrow$

0003–004X/89/0102–0191$02.00

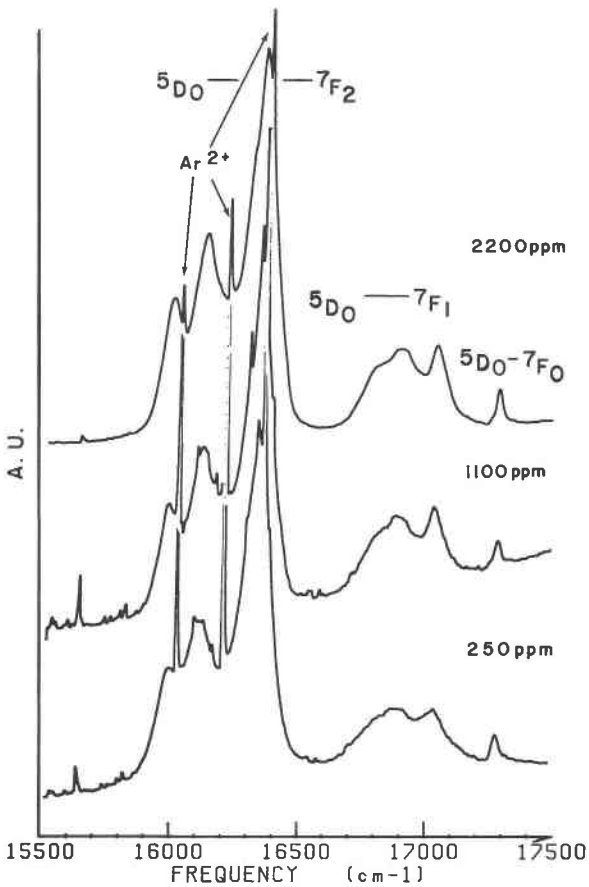

Fig. 1. Emission spectra of Eu^{3+} in anorthite after excitation at 4658 Å. These spectra were recorded at 300 K. For each spectrum, the concentration of Eu in the sample is indicated. (A.U.: arbitrary units.)

$^5D_0$ (absorption)) are forbidden. However, in a crystal, the mixing between wavefunctions of different J (J mixing) partially removes this interdiction. Because these two levels are nondegenerate, only one such transition can exist and be observed per site. The number of such transitions corresponds to a minimum number of different environments (or sites) of Eu^{3+}. Prather (1961) has tabulated the splitting of the levels as a function of their degeneracy in the free ions and the symmetry of the crystal field. Moreover, the study of the number and the intensities of the $^5D_0 \rightarrow {}^7F_1$ and $^5D_0 \rightarrow {}^7F_2$ transitions provides some insights on the environment of the ion.

Preparation of the samples

The anorthites studied were synthesized hydrothermally at 650 °C and 1.0 kbar for a duration of 14–21 d. The starting material was a dehydrated gel obtained from a stoichiometric mixture of aluminum nitrate, calcium nitrate, and colloidal silica (Ludox As-40, from which Na^+ has been removed by exchange). The stoichiometry of the starting material was checked by wet-chemical analysis. Eu^{3+} was added as a chloride in solution.

After hydrothermal synthesis the mineral and the solution were separated, and the mineral was carefully washed using nitric solution (pH = 2) to avoid adsorption of Eu^{3+} on the surface of the sample. The powder was then heated at about 1050 °C in air for 3 to 4 d to insure homogenization. The quality of the products was monitored by X-ray diffraction and optical observation; no other phase has been observed.

Optical measurements

The samples were compacted and cemented with a nonfluorescent glue. Although some measurements were carried out at 300 K (room temperature), most of them were done at 77 K by immersion of the samples in liquid N_2. The excitations were performed either using the 4658-Å violet line of an Ar-ion laser or, for site-selective excitation into $^5D_0$ level, with a tunable dye laser pumped by a N_2 pulsed laser (Jobin-Yvon).

The fluorescence was analyzed by a double monochromator (PHO Coderg) spectrometer driven by a computer that collected and processed the data. The time-resolved spectroscopy was performed by means of a digital oscilloscope (Tektronix 2400) coupled with the computer.

Experimental results

Emission spectra at 300 K

The emission spectra were obtained at room temperature after excitation by the 4658-Å line (30 mW). Three representative spectra of the $^5D_0 \rightarrow {}^7F_{0,1,2}$ transitions are reported in Figure 1. They correspond to different Eu-doped anorthites. The composition studied by Morris (1975) is included in the explored composition range. For samples containing less than 2500 ppm, no significant variation of the spectra is noted. They display the same features: three groups of broad lines corresponding respectively to the $^5D_0 \rightarrow {}^7F_0$, $^5D_0 \rightarrow {}^7F_1$, and $^5D_0 \rightarrow {}^7F_2$ transitions as indicated in Figure 1. The electric dipole $^5D_0 \rightarrow {}^7F_2$ transitions are the most intense, suggesting that the Eu^{3+} ions occupy sites with a very low symmetry. Such spectra look like those well known for Eu-doped glasses (see, for instance, Hufner, 1978; Brecher and Riseberg, 1980) in which the broad inhomogeneous lines correspond to sites forming large populations. In this study, however, the X-ray patterns indicate crystalline structure; therefore, lines may correspond to the summation of several spectra, each associated with a well-defined Eu^{3+} site.

Emission spectra at 77 K

For better resolution and understanding, the fluorescence was also observed at 77 K. One emission spectrum is illustrated in Figure 2a. In contrast to glasses, the broad bands are now resolved into numerous lines. Thus, the broad lines observed at 300 K result, partly, from the summation of several spectra corresponding to different sites. Figure 2b shows in detail the $^5D_0 \rightarrow {}^7F_0$ spectral range where three well-defined transitions with maxima at about 17274, 17280, and 17304 cm^{-1} are observed on a broad band. In the spectral region of the $^5D_0 \rightarrow {}^7F_1$ transitions, twelve lines of linewidth generally greater than 20 cm^{-1} are identifiable; their positions are indicated in Figure 2a. We have shown that the intense line centered at 17040 cm^{-1} and the three reported $^5D_0 \rightarrow {}^7F_0$ transitions are due to the emission of sites selectively excited in the $^5D_2$ level with the monochromatic line used. Be-

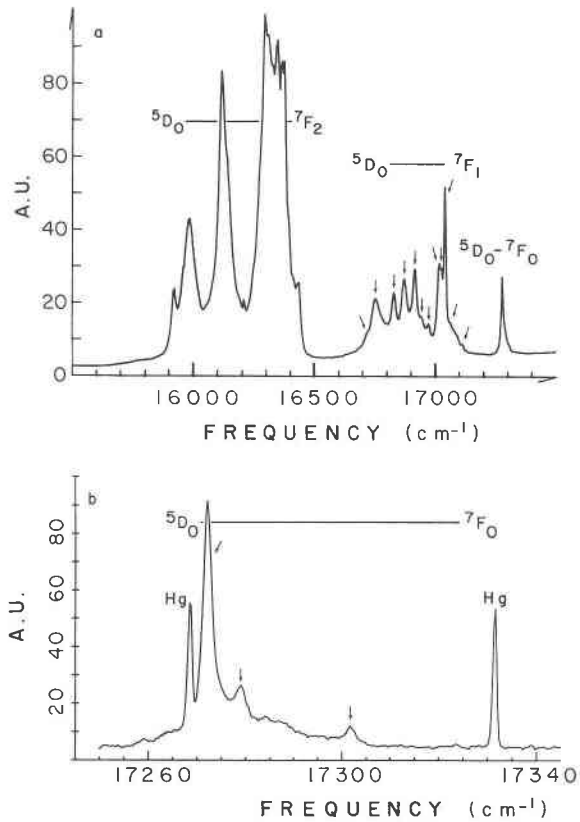

Fig. 2. (a) Emission spectrum of Eu^{3+} at 77 K after excitation at 4658 Å. The arrows indicate the $^5D_0 \rightarrow {}^7F_1$ transitions. (b) $^5D_0 \rightarrow {}^7F_0$ spectral range; the $^5D_0 \rightarrow {}^7F_0$ transitions are marked. Mercury emission lines are used as references. (A.U.: arbitrary units.) These spectra correspond to an anorthite containing 1100 ppm Eu^{3+}.

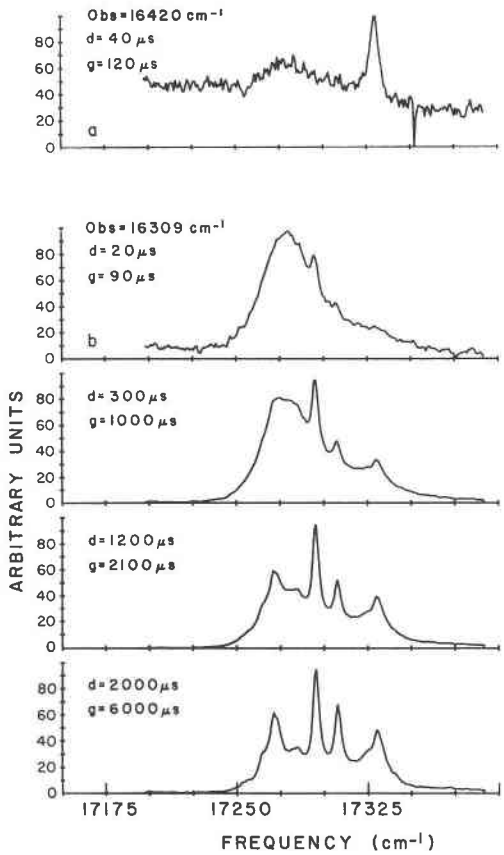

Fig. 3. (a) Time-resolved excitation spectrum monitored at 16420 cm^{-1}. The sample contains 1100 ppm Eu^{3+}. (b) Set of time-resolved excitation spectra monitored at 16309 cm^{-1}. These spectra were performed at 77 K. The delays (d) and the gates (g) are indicated for each spectrum.

cause there are four different Ca^{2+} sites in anorthite (Wainwright and Starkey, 1971), if Eu^{3+} substitutes for Ca^{2+} in every site, four lines should be observed in the $^5D_0 \rightarrow {}^7F_0$ region. The complete splitting of the levels is expected because of the $C1$ symmetry of these four large sites. Thus, the twelve reported $^5D_0 \rightarrow {}^7F_1$ transitions would be consistent with an incorporation of Eu^{3+} in the four sites. However, with the observed $^5D_0 \rightarrow {}^7F_0$ transitions being due to accidental selective excitations, the interpretation of this region of the spectra, in terms of number of sites, would be difficult and would remain doubtful. But the underlying broad band still indicates the presence of numerous sites.

Time-resolved spectroscopy under selective excitation

To obtain more insights into the distribution of Eu^{3+} in anorthite, it was necessary to use a systematic selective excitation. All of these experiments were conducted at 77 K. At first, we performed the excitation spectra to determine the $^7F_0 \rightarrow {}^5D_0$ resonance frequency of the different sites. Then using the appropriate excitation line, one subset of ions (one site) may specifically be excited, and only the transitions from the $^5D_0$ to the lower levels of this subset will be observed. But site-to-site energy transfers and accidental degeneracies can still broaden the lines. As will be discussed, the site-selective excitation lines are so close and the fluorescence so weak that it was necessary to use time-resolved techniques that permit a recording of the fluorescence after decay of the excitation line.

Excitation spectra. Excitation spectra were monitored at some predetermined frequencies of intense $^5D_0 \rightarrow {}^7F_2$ emission; the excitation line was continuously varied between 17200 and 17390 cm^{-1}. One should observe, immediately after excitation at some wavenumber, an intense narrow emission line indicating a selective excitation of a site emitting at the frequency of observation (see Fig. 3a). But most of the spectra exhibit a particular feature. Such a characteristic set of time-resolved spectra is shown in Figure 3b; the observation frequency is 16309 cm^{-1}. For any line between 17250 and 17380 cm^{-1}, we observe an excitation. The most efficient lines are around 17275 cm^{-1}. For lower energy, the efficiency decreases rapidly, whereas higher-energy lines become slowly inefficient.

TABLE 1. Summary of the experimental results

		Energy relative to $^7F_0$					Energy relative to $^7F_0$		
$^5D_0$ levels	$^5D_0 \rightarrow {}^7F_1$ transitions	$^7F_1$ levels	$^7F_1$ barycenters	B^2_M	$^5D_0$ levels	$^5D_0 \rightarrow {}^7F_1$ transitions	$^7F_1$ levels	$^7F_1$ barycenters	B^2_M
	17012	253				17124 B′			
F 17265.0	16900	365	371	699		17088 B″	221		
	16770	495				16970 B			
					B″ 17309.0	16928 B″	381	387	976
	17032 C					16854 B′			
	17008 E, E1	262	372 E1	566		16800 B′			
	16930 E	340				16750 B″	559		
E 17270.0	16906 C								
	16866 E1	404				17126 B′			
	16820 E1	450	377 E	791		17110 I	214		
	16742 E, C	528			I 17314.0	16964 I	350	398	1224
						16924 B″ ?			
	17040	233				16684 I	630		
C 17273.0	16914	359	375	870					
	16740	533			H 17325.0				
	17016	265				17160 D	169		
A 17281.0	16970	311	382	947		17144 P?			
	16712	569				17130 †			
						17000 †			
G 17281.9					D 17329.0	16970 †		392	1180
						16948 P?			
	17040	254				16892 D	437		
	17012 B?					16758 D	571		
L 17293.7	16856	438	410	832		16700 *P?			
	16756	538				16660 †			
	17124 B′	181				17164 De			
	17080 B					17144 P	192		
	16970 B				P 17335.5	16958 P	378	396	1233
B′ 17304.6	16926 B″		378	1002		16897 D			
	16854 B′	451				16768 D?			
	16800 B′	505				16718 P	618		
	16740 *B?								
					J 17345.0				
	17124 B′								
	17088 B″					17162	199		
	17080 B	226			K 17360.5	17052	309	411	1602
	16970 B	338				16636	724		
B 17307.6	16926 B″		379	1020					
	16854 B′								
	16800 B′								
	16758 B″								
	16736 B	572							

Note: For each recognized excitation line (noted as $^5D_0$), the $^5D_0 \rightarrow {}^7F_1$ transitions observed after selective excitation and their attribution are indicated. For each site, the $^7F_1$ levels and their barycenter relative to the $^7F_0$ and the parameter B^2_M are calculated. The energy is indicated in cm^{-1}. Transitions marked with * indicate a broad band; ? indicates uncertain attribution; † indicates transitions corresponding to the site H and a non–directly characterized site (see text about spectra D).

However, the resulting emission decays rapidly and, after a delay of about 300 μs, the spectra usually show two or three specific excitation lines. The presence of either a broad population of asymmetric Eu^{3+} sites or lattice defects may explain this large spectral range of excitation. Nevertheless, these unusual excitation spectra remain partially unexplained. Moreover, this large range of the excitation lines does not allow us to recognize possible site-to-site energy transfers that can explain this apparent nonselectivity. Therefore, the excitation lines for which a selective emission is observed on the delayed spectra are considered to be specific of some sites. These sites either have an emission line corresponding to (or close enough to) the monitoring frequency, or de-excite by transfer on a site emitting at the frequency of observation. To insure the characterization of all sites, excitation lines were sought for in the $^7F_0 \rightarrow {}^5D_0$ spectral range by performing careful emission spectra by scans of the $^5D_0 \rightarrow {}^7F_2$ region for different excitation lines separated by only 2 cm^{-1}.

Fifteen $^7F_0 \rightarrow {}^5D_0$ transitions have been identified. Their wavenumbers (see Table 1) are surprisingly close, sometimes separated by less than 5 cm^{-1}. This observation explains the nonperfect selectivity noted for the excitation spectra. Each identified excitation line ($^7F_0 \rightarrow {}^5D_0$ transition) is labeled by a letter that is also used to designate its associated Eu^{3+} site.

For every recognized $^7F_0 \rightarrow {}^5D_0$ transition, a set of time-resolved spectra has been recorded in the spectral region of 16500–17200 cm^{-1}. Because the spectra obtained for anorthites containing between 100 and about 2500 ppm

Eu are identical, we have chosen to study, in detail, a sample containing 1100 ppm. At this middle concentration, the intensity of fluorescence is usually strong enough to get good spectra. For lower concentrations, the intensities rapidly become too weak to record spectra free of noise.

$^5D_0 \rightarrow {}^7F_1$ transitions. One characteristic set of such time-resolved spectra is shown in Fig. 4a. It displays the time dependence of the intensity of fluorescence for the $^5D_0 \rightarrow {}^7F_1$ transitions. Immediately after the excitation, a broad and intense fluorescence seems to overlay the $^5D_0 \rightarrow {}^7F_1$ transitions (the same phenomenon is observed in the region of 15500–16500 cm^{-1}). Since this broad fluorescence decreases rapidly, the delayed spectra usually display well-defined lines with a linewidth of about 10–15 cm^{-1} (of the same order of the slitwidth used). On some spectra (Fig. 4a), the early emission presents several maxima, centered in the typical region of Eu^{3+} transitions, suggesting it is due to Eu^{3+} ions in sites forming a large and continuous population (as in glasses). Few delayed spectra are simple, for example, site F in Figure 4a, and composed of only three lines. They indicate a complete splitting of the $^7F_1$ level by a field of low symmetry. The others are more complex (Fig. 4b) and result from the superposition of several spectra, each corresponding to a different site. This complexity is probably due to the close frequencies of the $^5D_0$ levels, but it also may be due to site-to-site energy transfers as already suggested. All the observed $^5D_0 \rightarrow {}^7F_1$ transitions are reported in Table 1 and represented as a function of the $^5D_0$ level (or excitation line) in Figure 5.

A careful study of the different line evolutions in each set of spectra allows the recognition of the transitions corresponding to the same site (see Table 1 and Fig. 5). As shown in Figure 5, the spectra recorded after excitation by the line labeled E (17270 cm^{-1}) correspond to three sites; one of them named C is selectively excited by the 17273 cm^{-1} line. Also in Figure 5 (and Fig. 4b), the spectrum denoted D is composed of ten lines corresponding to four sites: P, D itself, H, and a fourth site yet to be characterized by its excitation line; site H was determined from a study of the $^5D_0 \rightarrow {}^7F_2$ transitions. The $^5D_0 \rightarrow {}^7F_1$ transitions of the sites G, H, and J were too weak to be correctly identified; nevertheless, these sites were characterized by the $^7F_0 \rightarrow {}^5D_0$ transitions in the excitation spectra.

Every characterized site spectrum shows three $^5D_0 \rightarrow {}^7F_1$ transitions indicating a low-symmetry crystal field. As can be seen in Figure 5, the splitting of the $^7F_1$ level increases with the energy of the $^5D_0$ level above $^7F_0$. For the site F, the splitting is only 242 cm^{-1}, whereas for the site K it is as large as 526 cm^{-1}; this indicates an increase of the crystal field.

$^5D_0 \rightarrow {}^7F_2$ transitions. The large number and low symmetry of the sites and the broad linewidth of the $^5D_0 \rightarrow {}^7F_2$ transitions resulted in important overlaps of the peaks. Therefore, it was not possible to use these transitions to obtain more insights into the crystal field. The set of all such transitions is represented versus the wavenumber of the excitation lines in Figure 6. For these spectra, the transitions specific to the sites G, H, and J are well-defined; as indicated, the broad fluorescence bands are also observed, and the increase of the crystal field can be distinguished. The strong intensities of these lines relative to the $^5D_0 \rightarrow {}^7F_1$ confirm a very low symmetry of the crystal field.

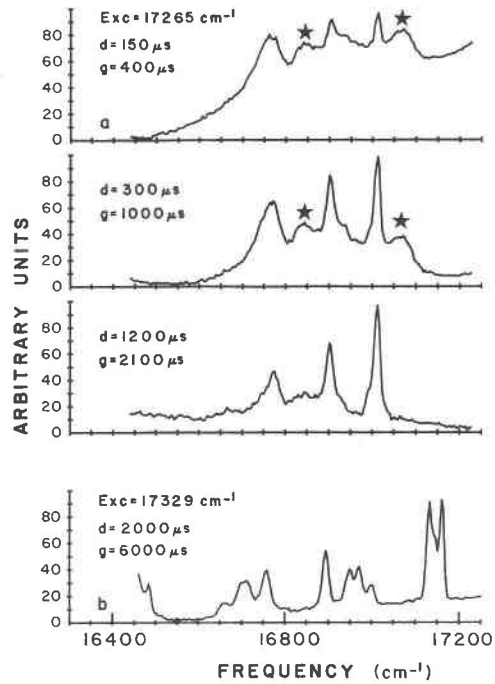

Fig. 4. (a) Emission time-resolved spectra of the site F after selective excitation in the $^5D_0$. The stars indicate the broad bands of early fluorescence. (b) Emission time-resolved spectrum after excitation at 17329 cm^{-1}. This spectrum results from the superposition of lines associated with different sites (see text).

In summary, using the 15 predetermined excitation lines, 17 different sites have been distinguished.

Discussion

All reported spectra show two different types of fluorescence. One is characterized by early and broad bands that decay rapidly, and the other by well-defined transitions. Both will be considered separately.

The broad band fluorescence

These bands of short decay time appear in the $^5D_0 \rightarrow {}^7F_1$ and $^5D_0 \rightarrow {}^7F_2$ spectral ranges and are similar to those observed for doped glasses in which Eu^{3+} ions are dispersed in a wide and continuous population of sites. Thus, we think that this fluorescence is due to Eu^{3+} ions scattered in sites forming such a "glasslike" population. Its structural interpretation is difficult. However, Eu^{3+} ions trapped in defects, and not in crystallographically repeated sites, should form such a population. Among the possible defects are cleavages, twin planes, dislocations, or

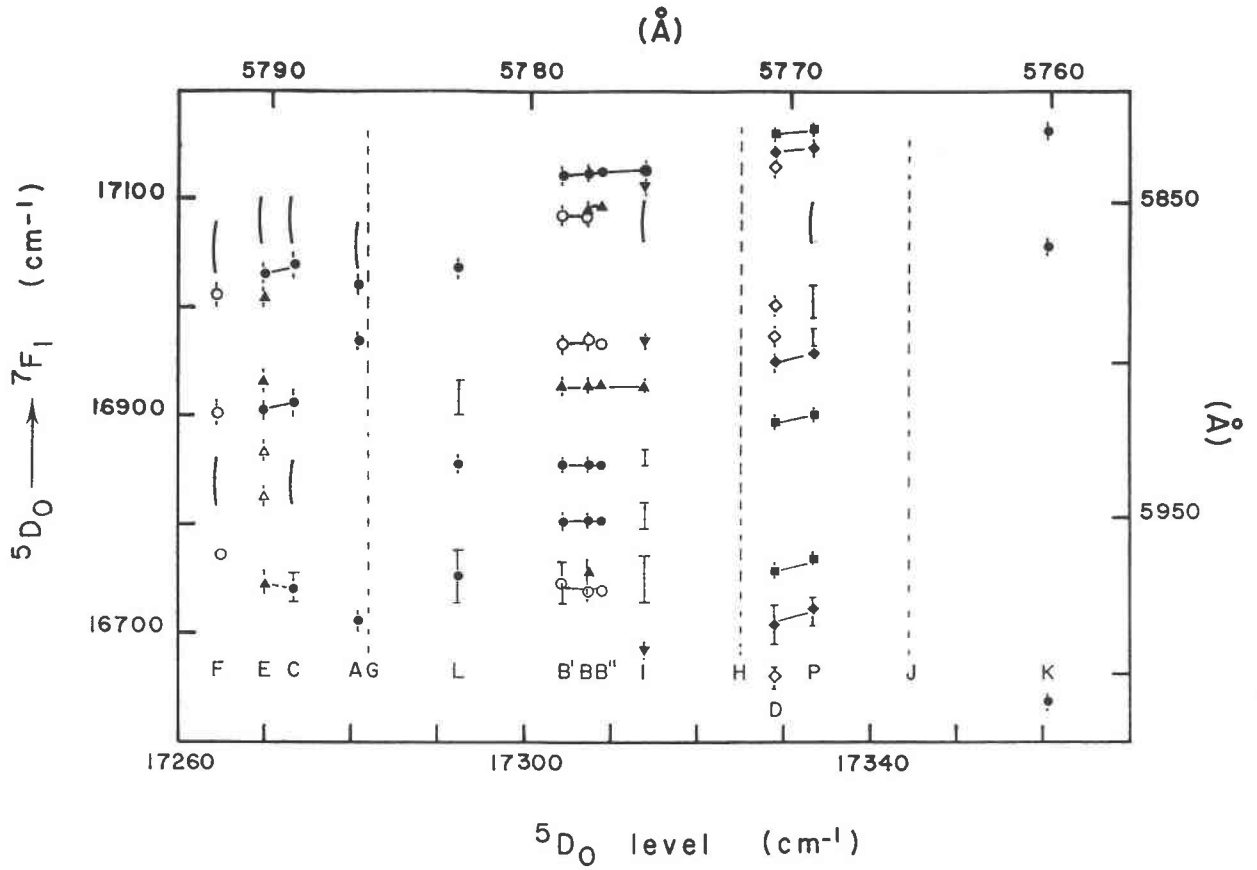

Fig. 5. Observed $^5D_0 \rightarrow {}^7F_1$ transitions vs. the corresponding excitation lines. The arcs indicate the broad bands of early fluorescence; the bars designate broad but weak bands that can correspond to transitions from other sites than the one excited. For a given excitation line, a given symbol indicates the transitions corresponding to the same site; the solid lines join transitions common to different spectra.

join boundaries. These likely are favorable zones to trap Eu^{3+} ions in numerous different environments that on the average can be considered as a continuous glassy population. Thus, we believe that some of the Eu^{3+} ions are trapped in such defects and not in the Ca^{2+} sites.

Fluorescence of the narrow lines

Seventeen low-symmetry or asymmetric sites have been characterized. Their structural interpretation remains difficult because only four different Ca^{2+} sites are defined in anorthite (Wainwright and Starkey, 1971), and moreover, an exact quantitative description of the crystal field is not possible on the basis of the available data. The first difficulty can easily be overcome, because fluorescence spectroscopy is a local probing method able to differentiate very similar structures indistinguishable by X-ray diffraction. But this explanation does not exclude inhomogeneous deformations of the substituted sites that would create new and more numerous sites.

As previously noted, the higher that the $^5D_0$ level is above $^7F_0$, the stronger the crystal field. In Table 1, the positions of the $^7F_1$ level barycenters, relative to $^7F_0$, are calculated on the basis of the attributions. It is easy to see the correlation between the $^7F_1$ and $^5D_0$ levels. The complete description of the crystal field would require the knowledge of numerous $^{2S+1}L_J$ levels that are not available. But neglecting the J mixing, and using a crude approximation, the energies of the $^7F_1$ Stark levels relative to their barycenter can be expressed by the relations (Dexpert-Ghys, 1979)

$$\begin{aligned} E(1) &= 0.2B_0^2 \\ E(2) &= -0.1B_0^2 + 0.245B_2^2 \\ E(3) &= -0.1B_0^2 - 0.245B_2^2, \end{aligned}$$

where E(1), E(2), and E(3) represent the energy (cm^{-1}) of the Stark levels and B_0^2 and B_2^2 are the experimental adjustable phenomenological parameters, B_q^k, defined by Wybourne (1965) to describe the crystal field. Then, an average parameter B_M^2 can be designed to measure the intensity of the crystal field:

$$B_M^2 = [2(B_2^2)^2 + (B_0^2)^2]^{1/2}.$$

With this average parameter, the problems of assignment of the levels with respect to the symmetry are avoided.

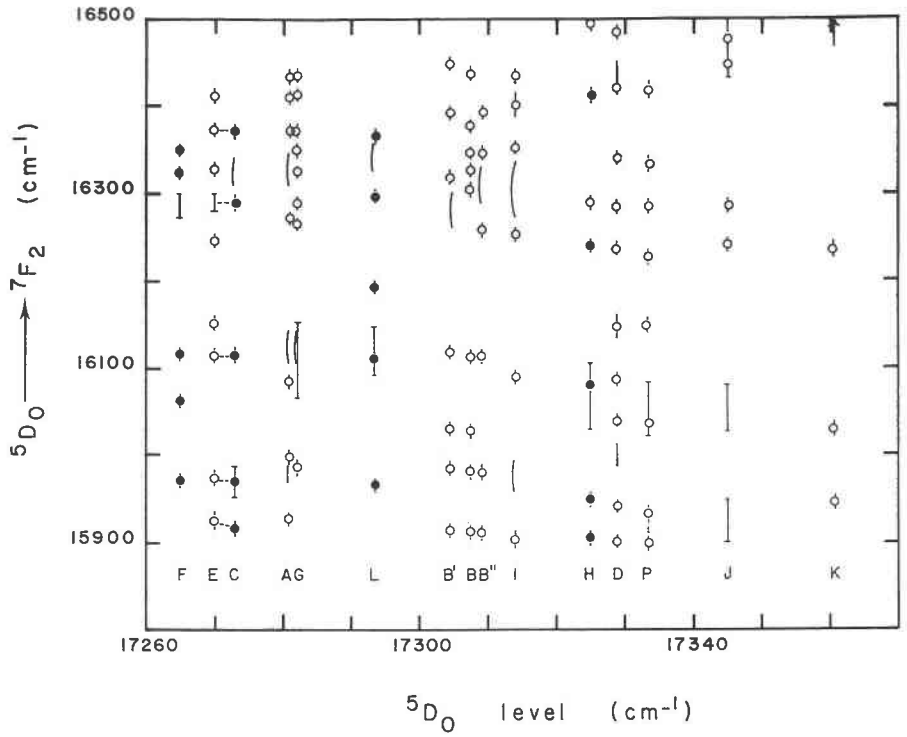

Fig. 6. $^5D_0 \rightarrow {}^7F_2$ transitions observed for the different excitation lines. Arcs and bars are as in Fig. 5; for a given excitation frequency, solid symbols indicated transitions corresponding to the same site.

The values of this parameter are reported in Table 1. When plotted as a function of the $^5D_0$ level (Fig. 7), three linear trends labeled I, II, and III can be defined. Such a trend has been described by Dexpert-Ghys and Piriou (1987) for Eu^{3+} in glasses and interpreted by a variation of the crystal field in a population of related sites. For example, for a given angular environment, the crystal field increases as the cation-ligand distances decrease. With this hypothesis, we may expect the $^5D_0$ energy to be that of the free ion for an infinite cation ligand-distance, i.e., for a null crystal field. For each trend drawn in Figure 7, the relative energy estimated at $B^2_M = 0$, by simple extrapolation, is only slightly smaller (by 20–40 cm^{-1}) than the value of 17265 cm^{-1} given by Crosswhite and Moos (1967). This proves that the interpretation is at least self-consistent.

In anorthite, Wainwright and Starkey (1971) described four different Ca sites: Ca(000), Ca(zi0), Ca(z00), and Ca(0i0). The Ca(z00) and Ca(0i0) sites are similar: they have the same coordination number (7) and close angles

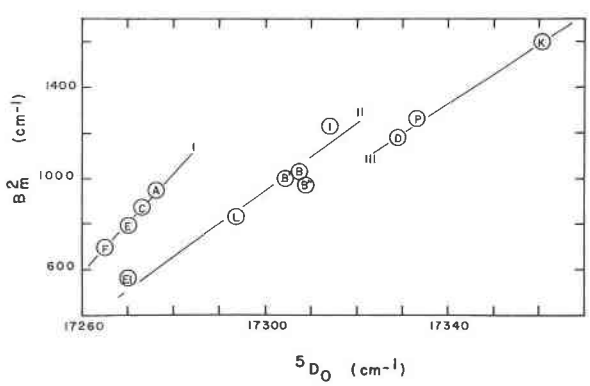

Fig. 7. Variation of the parameter B^2_M with the $^5D_0$ energy relative to the $^7F_0$ level.

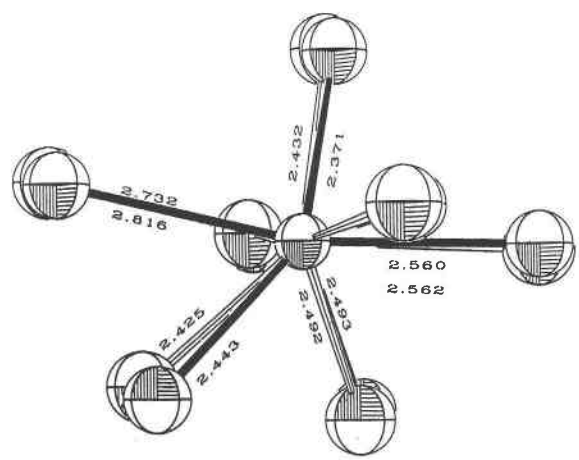

Fig. 8. Comparison between the Ca(z00) and Ca (0i0) sites of anorthite described by Wainwright and Starkey (1971). The Ca^{2+} ions are superposed. The black bonds correspond to Ca(z00) and the white ones to Ca (0i0).

and bond lengths as shown in Figure 8. On the other hand, the Ca(000) and Ca(*zi*0) sites are significantly different by their bond lengths, angles, and coordination number (6 and 7, respectively). The mean bond lengths R(Ca–O) are 2.453 ± 0.119, 2.490 ± 0.132, 2.502 ± 0.188, and 2.533 ± 0.188 Å for Ca(000), Ca(*z*00), Ca(0*i*0), and Ca (*zi*0), respectively.

As the crystal field increases from trend I to trend III, we assume that trend I corresponds to sites similar to Ca(*zi*0) (longest Ca–O distances) and that trend III to sites derived from Ca(000) (shortest Ca–O distances), while we suggest that trend II corresponds to sites related to Ca(*z*00) and Ca(0*i*0). We neglect the coordination number of the ions because its influence on the intensity of the crystal field cannot be defined a priori.

Bearing in mind that the present method of the local probe is very sensitive, the large number of substitutional sites is interpreted by inhomogeneous deformations of the substituted sites. Ca^{2+} sites in anorthite tend to be smaller than Na^{+} sites in albite (Smith, 1974) because of the larger ionic potential of Ca^{2+}. The silicate framework collapses more around Ca^{2+} than around Na^{+}. The unique Na^{+} site in albite is replaced by four Ca^{2+} sites because the framework deformation is not homogeneous. As the ionic potential of Eu^{3+} is greater than that of Ca^{2+}, the same process is assumed for the substitution of Eu^{3+} for Ca^{2+}. The coupled substitution necessary for electronic balance may also contribute to the deformation of the network. The framework collapses irregularly yielding several Eu^{3+} sites for each original Ca^{2+} site. Such deformations of the framework are consistent with the relationship between the tetrahedral angles (O–(Si,Al)–O) and the charge of the nontetrahedral cation in the feldspars, as proposed by Megaw et al. (1962). As the charge of these cations increases from +1 to +2, the distortion of the tetrahedral units increases by narrowing and widening of the angles. This results in modifications of the silicate network. An extrapolation of this relationship for trivalent cations shows even more distorted tetrahedrons and, furthermore, would imply deformations of the framework. Such modifications could create new sites and even yield defects if the stresses are too high.

Conclusions

The features of the reported spectra indicate two main populations of Eu^{3+} sites in anorthite. Some of the ions are trapped in extended defects such as possibly twin and cleavage planes, whereas the rest substitute for Ca and may be divided in three subsets. The ratio between these populations could not be determined in the present study. Despite similar ionic radii, the substitution of Eu^{3+} for Ca^{2+} is accompanied by deformations of the sites probably by collapsing of the aluminosilicate framework around the sites. These results are in partial agreement with those of Morris (1975), but we show that a fraction of the REE^{3+} is probably trapped in defects and does not substitute for Ca^{2+}. For the studied concentrations, which are relatively high compared to those of natural samples, the results are compatible with the two-stage models of incorporation of REEs previously described.

This study also provides some insights into the partition of the REE^{3+} ions in plagioclases. The partition coefficients of the REE^{3+} ions between plagioclase and magmatic liquid ($D^{pl,li}_{REE}$) are generally small (0.01 to 0.10) with the exception of $D^{pl,li}_{Eu}$ and do not vary significantly with the atomic number of the ions. These small variations can be interpreted on the basis of the proposed distribution of Eu^{3+} modeling the distribution of the other REE^{3+} ions. We can expect that the REE^{3+} ions will be randomly trapped in the defects, thus leading to nonselectivity among them. Each substituted site may exhibit some selectivity, but this selectivity will be different from site to site because of the variations of the size of the sites and of the ionic radii. Therefore, an overall nonselectivity could be expected.

If the Ca^{2+} sites are large enough to receive the REE^{3+}, other parameters limit the process. The aluminosilicate three-dimensional network is particularly rigid, and the proposed deformation of the framework induced by the substitution of Ca^{2+} by REE^{3+} is probably one of the limiting factors. The charge-compensation mechanism (not discussed here) will be another limiting factor.

The scarcity of available data does not permit us to express rules controlling the REE^{3+} partitioning in minerals. But we can say that the dispersion of REE^{3+} ions in numerous sites as described here explains the nonselectivity of the plagioclases among these elements. In zircon, the REE^{3+} ions are localized in the relatively small Zr^{4+} site (Reynolds et al., 1972; Ball, 1982); this mineral strongly fractionates the heavy and smallest REE^{3+}. In apatite, the REE^{3+} ions substitute for Ca^{2+}, and the intermediate REE^{3+} ions are preferentially incorporated. Notice that, in both cases, the REE^{3+} ion that gives the better steric fit in the mineral structure substitutes preferentially for the major element (see Nagasawa, 1966). So it seems that if REE^{3+} ions are localized in a well-defined site, the mineral shows some selectivity. On the other hand, if no significant fractionation is noticed, a broad population of available sites (defects or modified structural sites) may be expected. A better knowledge of the mechanisms of incorporation of the REE^{3+} ions would facilitate explanation of their geochemical behavior. The method used appears to be one of the most powerful to investigate the problem and should be applied in future studies.

Acknowledgments

We are particularly grateful to Professor P. Caro and Dr. J. Dexpert-Ghys (CNRS, Meudon, France) for their support and fruitful discussions during this work. We also thank Professors M. Julian, G. V. Gibbs and P. H. Ribbe (Virginia Polytechnic Institute) for their comments to improve the readability of the text.

References cited

Ball, D. (1982) The paramagnetic resonance of Nd^{3+} and Yb^{3+} in zircon structure silicates. Physica Status Solidi (b), 111, 311–320.

Brecher, C., and Riseberg, L.A. (1980) Laser-induced fluorescence line narrowing in rare-earth doped glasses: Spectroscopic variations and

their structural implications. Journal of Non-Crystalline Solids, 40, 469–480.

Caro, P. (1976) Structure électronique des éléments de transition, l'atome dans le cristal, 204 p. Presse Universitaire de France, Paris.

Crosswhite, H.M., and Moos, H.W. (1967) Crystal spectroscopy at the Johns Hopkins University. In H.M. Crosswhite and H.W. Moos, Eds., Optical properties of ions in crystals, p. 3–33. Wiley, New York.

Dexpert-Ghys, J. (1979) Etude au moyen de la sonde structurale Eu^{3+} des sites cristallographiques des lanthanides dans quelques oxydes. Thèse d'Etat Orsay, France.

Dexpert-Ghys, J., and Piriou, B. (1987) Etude spectroscopique de l'ion Eu^{3+} dans un verre alumino-boro-silicate. Réunion des silicates d'aujourd'hui et demain: du cristal au liquide. Société des Hautes Températures et Réfractaires—Société Française de Minéralogie et Cristallographie (Paris).

Fahmi, D. (1986) Contribution à la structure de quelques matrices cristallines phosphatées par spectroscopie optique de l'ion Eu^{3+}. Thèse d'Université, Paris.

Harrison, W.J. (1978) Rare element partitioning between garnets, pyroxenes, and melts at low trace element concentration. Carnegie Institution of Washington Year Book 77, 682–689.

——— (1981) Partition coefficients for REE between garnets and liquids: Implications of non-Henry's law behaviour for models of basalt origin and evolution. Geochimica et Cosmochimica Acta, 45, 1529–1544.

Hufner, S. (1978) Optical spectra of transparent rare earth compounds, 237 p. Academic Press, New York.

Jensen, B.B. (1973) Patterns of trace elements partitioning. Geochimica et Cosmochimica Acta, 37, 2227–2242.

Megaw, H.D., Kempster, C.E.J., and Radoslovich, E.W. (1962) The structure of anorthite, $CaAl_2Si_2O_8$: II. Description and discussion. Acta Crystallographica, 15, 1017–1035.

Morgan, J.W., and Wandless, G.A. (1980) Rare earth elements distribution in some hydrothermal minerals: Evidence for crystallographic control. Geochimica et Cosmochimica Acta, 44, 973–980.

Morlotti, R., and Ottonello, G. (1982) Solution of rare earth elements in silicate solid phases. Henry's law revisited in light of defect chemistry: Garnet, clinopyroxene, and plagioclase. Physics and Chemistry of Minerals, 8, 87–97.

Morris, R.V. (1975) Electron paramagnetic resonance study of the site preferences of Gd^{3+} and Eu^{2+} in polycrystalline silicate and aluminate minerals. Geochimica et Cosmochimica Acta, 39, 621–634.

Nagasawa, H. (1966) Trace element partition coefficient in ionic crystals. Science, 152, 767–769.

Piriou, B., Fahmi, D., Dexport-Ghys, D.J., Taitai, A., and Lacout, J.L. (1987) Unusual fluorescence properties of Eu^{3+} in oxyapatites. Journal of Luminescence, 39, 97–103.

Prather, J.L. (1961) Atomic energy levels in crystals. N.B.S. Monography, 19, 84 p.

Reynolds, R.W., Boatner, L.A., Finch, C.B., Chatelain, A., and Abraham, M.M. (1972) EPR investigations of Er^{3+}, Yb^{3+}, and Gd^{3+} in zircon structure silicates. Journal of Chemical Physics, 56, 5607–5625.

Smith, J.V. (1974) Feldspar minerals—1. Crystal structures and physical properties, 627 p. Springer-Verlag, Berlin.

Wainwright, J.E., and Starkey, J. (1971) A refinement of the structure of anorthite. Zeitschrift für Kristallographie, 133, 75–84.

Wybourne, B.G. (1965) Spectroscopic properties of ions in crystals, 236 p. Wiley, New York.

Manuscript received March 4, 1988
Manuscript accepted September 6, 1988